Spin reorientation in α-Fe_2O_3 nanoparticles induced by interparticle exchange interactions in α-Fe_2O_3/NiO nanocomposites

C. Frandsen,[1,*] K. Lefmann,[2,3,4] B. Lebech,[2,4] C. R. H. Bahl,[4,5] E. Brok,[1,6] S. N. Ancoña,[4,†] L. Theil Kuhn,[4,5] L. Keller,[7] T. Kasama,[6] L. C. Gontard,[6,‡] and S. Mørup[1]

[1]*Department of Physics, Technical University of Denmark, DK-2800 Kgs. Lyngby, Denmark*
[2]*Nano-Science and eScience Centers, Niels Bohr Institute, University of Copenhagen, Universitetsparken 5, DK-2100 Copenhagen Ø, Denmark*
[3]*European Spallation Source, Lund, Sweden*
[4]*Materials Research Division, Risø DTU, Technical University of Denmark, DK-4000 Roskilde, Denmark*
[5]*Fuel Cells and Solid State Chemistry Division, Risø DTU, Technical University of Denmark, DK-4000 Roskilde, Denmark*
[6]*Center for Electron Nanoscopy, Technical University of Denmark, DK-2800 Kgs. Lyngby, Denmark*
[7]*Laboratory for Neutron Scattering, Paul Scherrer Institute, CH-5232 Villigen PSI, Switzerland*

(Received 30 March 2011; revised manuscript received 14 October 2011; published 22 December 2011)

We report that the spin structure of α-Fe_2O_3 nanoparticles rotates coherently out of the basal (001) plane at low temperatures when interacting with thin plate-shaped NiO nanoparticles. The observed spin reorientation (up to $\sim 70^\circ$) in α-Fe_2O_3 nanoparticles has, in appearance, similarities to the Morin transition in bulk α-Fe_2O_3, but its origin is different—it is caused by exchange coupling between aggregated nanoparticles of α-Fe_2O_3 and NiO with different directions of easy axes of magnetization.

DOI: 10.1103/PhysRevB.84.214435 PACS number(s): 75.75.−c, 75.50.Tt, 75.25.−j

I. INTRODUCTION

Magnetic coupling between different materials in direct contact is a subject of considerable interest. Exchange coupling between a ferro- or ferrimagnetic material and an antiferromagnetic material in, for example, thin film structures can lead to exchange bias,[1–4] which is a key ingredient in read heads in computers. The spin structure at the interface has attracted much attention, and numerous experimental studies and theoretical models for exchange bias have been published.[2–4] In most of this work, the sublattice magnetizations of the antiferromagnetic material and the ferro- or ferrimagnetic material are assumed parallel at the interface, but in some experimental studies, it was surprisingly found that the sublattice magnetizations of the interacting materials may be perpendicular. The latter can be explained by a spin flop induced by the exchange field as proposed by Koon,[5] but anisotropic exchange interaction[6] and spin frustration at the interface may also play an important role.

In samples of antiferromagnetic nanoparticles in close proximity, magnetic interactions can also have a significant influence on the magnetic properties.[7] Antiferromagnetic particles have small magnetic dipole moments and therefore dipole interactions are negligible; yet, Mössbauer studies of antiferromagnetic nanoparticles of hematite (α-Fe_2O_3),[8–11] NiO,[12–14] and ferrihydrite[15] have shown that interparticle interactions between particles, prepared by drying aqueous suspensions, can result in a substantial suppression of the superparamagnetic relaxation. This has been explained by exchange interactions between surface atoms of neighboring particles.[8–11,16–18]

The exchange interaction between two neighboring particles p and q may be written

$$E_{\mathrm{ex}} = -\sum_{i,j} J_{ij}\, \vec{S}_i^{\,p} \cdot \vec{S}_j^{\,q}, \qquad (1)$$

where $\vec{S}_i^{\,p}$ and $\vec{S}_j^{\,q}$ are surface spins of the particles p and q, respectively, and J_{ij} is the exchange coupling constant. For simplicity, we consider only one sublattice of particle p interacting with one sublattice of the particle q. Equation (1) can then be written[11]

$$E_{\mathrm{ex}} = -J_{\mathrm{eff}}\, \vec{M}_p \cdot \vec{M}_q = -J_{\mathrm{eff}}\, M_p\, M_q \cos\beta, \qquad (2)$$

where $\vec{M}_p$ and $\vec{M}_q$ are the sublattice magnetization vectors of the particles p and q, respectively, J_{eff} is the effective exchange coupling constant, and β is the angle between $\vec{M}_p$ and $\vec{M}_q$.

The observation of strong exchange interactions in dried nanoparticle samples suggests that the drying actually brings the particles closely together and that the exact particle arrangement may include some kind of preferred orientation.[8–15,17] Oriented attachment has also been found in transmission electron microscopy studies of larger α-Fe_2O_3 particles with different morphologies.[19]

In this work, we have studied the influence of interactions between nanoparticles of NiO and α-Fe_2O_3 on the magnetic structure of α-Fe_2O_3. Our findings suggest that the interactions can lead to a spin reorientation in α-Fe_2O_3 nanoparticles out of the interface plane. We compare the studies of α-Fe_2O_3/NiO with studies of α-Fe_2O_3/CoO.

The crystal structure of α-Fe_2O_3 can be described in terms of alternating iron and oxygen layers stacked along the [001] axis of the hexagonal unit cell (see, e.g., Morrish[20]). The Fe layers order antiferromagnetically below the Néel temperature, $T_{\mathrm{N}} \approx 955$ K, such that the magnetization directions of neighboring Fe layers become antiparallel. The sublattice magnetization directions of α-Fe_2O_3 are confined to lie within the (001) plane above the Morin transition temperature, T_{M}, which in bulk α-Fe_2O_3 is 263 K. Between T_{N} and T_{M}, the two sublattices form a small canting angle of about 0.1° away from perfect antiferromagnetic alignment. Below T_{M}, the sublattice magnetization directions are rotated by 90° out of the (001) plane such that they become parallel to the [001] direction

with no canting. The Morin transition temperature decreases with decreasing particle size, and in α-Fe_2O_3 particles with diameters less than approximately 20 nm, there is no Morin transition above the temperature of liquid helium.[20,21]

NiO and CoO are face-centered cubic (fcc) antiferromagnetic materials with Néel temperatures of 523 K and 293 K, respectively. Within the (111) planes, the cations are ferromagnetically coupled, and adjacent (111) planes are antiferromagnetically coupled. In NiO, the common direction of the sublattice magnetization is within the (111) plane, whereas for CoO, it is a direction close to the $[\bar{1}\bar{1}7]$ axis.[22] However, for nanoparticles, the magnetic structure can be different from that of the bulk materials.[23]

Mössbauer studies of composites of nanoparticles of α-Fe_2O_3 mixed with NiO or CoO have shown some interesting results.[18,24] Mixing with NiO resulted in faster superparamagnetic relaxation of the α-Fe_2O_3 particles at finite temperatures, whereas mixing with CoO had the opposite effect. Well below the blocking temperature of α-Fe_2O_3 particles, a significant reorientation of the spin system of α-Fe_2O_3 was found in the α-Fe_2O_3/NiO sample, whereas no spin reorientation was found in the α-Fe_2O_3/CoO sample. It has also been shown that interactions between α-Fe_2O_3 nanoparticles with different crystallographic orientations, obtained by freeze-drying particle suspensions, can result in reorientation of the spin structure, such that the sublattice magnetization forms finite angles with the easy axes defined by the magnetic anisotropy.[17] In this paper, we present the results of a detailed investigation of the spin reorientation in α-Fe_2O_3/NiO nanocomposites by combined use of Mössbauer spectroscopy, neutron scattering, and transmission electron microscopy (TEM).

II. EXPERIMENTAL DETAILS

Nanoparticles of α-Fe_2O_3 (approximately spherical, ~8 nm in diameter) were synthesized by means of a gel-sol method.[25] NiO particles (plate-shaped, ~15 nm in diameter and ~2 nm thick) were prepared by annealing $Ni(OH)_2$ in air for 3 h,[18] and CoO particles (approximately spherical, 20 nm in diameter) were prepared by annealing Co-acetate in argon for 4 h.[18] All samples were characterized by x-ray diffraction and TEM. The α-Fe_2O_3 particles are from the same batch as those studied in Refs. 9 and 18, and the NiO particles are similar to those studied in Refs. 14 and 18.

A sample of pure 8-nm α-Fe_2O_3 nanoparticles with limited interparticle interaction was prepared as a ferrofluid, in which the particles in suspension were coated with oleic acid after intense ultrasonic treatment. A sample of interacting 8-nm α-Fe_2O_3 particles was prepared by freeze-drying a suspension of noncoated particles from the same batch.

Composites of α-Fe_2O_3/NiO and α-Fe_2O_3/CoO nanoparticles were prepared as reported in Ref. 18 by suspending 50 mg of each of these powders into 100 ml of distilled water. Within this, the particles were exposed to intense ultrasound for 15 minutes by use of an ultrasonic horn, with the aim to break apart agglomerates of particles and obtain a homogeneous mixture of the particles. The particles were then allowed to settle and dry at room temperature in an open petri dish. This procedure was repeated several times to obtain sufficient material for neutron diffraction experiments.

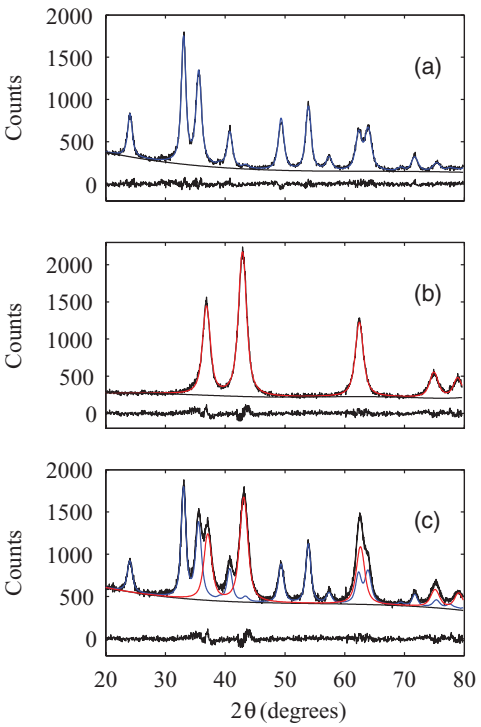

FIG. 1. (Color online) Rietveld refined x-ray diffraction data of (a) 8-nm α-Fe_2O_3 particles, (b) NiO nanoparticles, and (c) α-Fe_2O_3/NiO nanoparticle composite. The refinement of α-Fe_2O_3 is shown in blue/medium gray, that of NiO in red/dark gray, and the total refinement (c) in black.

Figure 1 shows Rietveld refined x-ray diffraction data (Cu Kα, $\lambda = 1.54$ Å) of (a) freeze-dried α-Fe_2O_3 nanoparticles, (b) NiO nanoparticles, and (c) α-Fe_2O_3/NiO nanoparticle composite. The refinement shows that the α-Fe_2O_3 and NiO samples are pure phases and that the particle sizes remain the same in the composite sample [Fig. 1(c)] as in the pure samples [Fig. 1(a) and 1(b), respectively].

The samples were studied by ^{57}Fe Mössbauer spectroscopy using constant acceleration spectrometers with sources of ^{57}Co in Rh. The spectrometers were calibrated using a 12.5 μm foil of α-Fe. Spectra were obtained at temperatures of 20–300 K using a closed-cycle helium refrigerator from APD Cryogenics. Cold neutron powder diffraction data were obtained at temperatures between 20 K and 300 K, using a wavelength of 4.20 Å, at the DMC diffractometer at the Swiss Spallation Neutron Source, SINQ, Paul Scherrer Institute. For all Mössbauer spectroscopy and neutron diffraction studies presented here, the samples were cooled to low temperatures (20 K) and then measured at increasing temperatures (35 K, 50 K, etc). However, we found no thermal hysteresis on the spin orientation by comparison of Mössbauer measurements of the α-Fe_2O_3/NiO sample obtained at same temperatures after cooling from 295 K and after heating from 20 K. TEM imaging was performed using JEOL 3000F and FEI Technai field-emission gun TEMs (300 keV) equipped with Gatan Imaging Filters. Elemental mapping was acquired using a three-window background-subtracted method with Gatan imaging filter.

III. RESULTS

A. Mössbauer spectroscopy

For studies of spin reorientation relative to the [001] axis in α-Fe_2O_3 nanoparticles, Mössbauer spectroscopy is a very useful technique. The electric field gradient in α-Fe_2O_3 is parallel to the [001] axis and the quadrupole shift, ε, is given by

$$\varepsilon = \varepsilon_0(3\cos^2\theta - 1)/2, \quad (3)$$

where $\varepsilon_0 = 0.20$ mm/s, and θ is the angle between the magnetic hyperfine field (antiparallel to the magnetic moment of the ion) and the [001] axis. Thus, the quadrupole shift changes from $\varepsilon = -0.10$ mm/s above the Morin transition temperature, where $\theta = 90^\circ$ to $\varepsilon = +0.20$ mm/s below T_M, where $\theta = 0^\circ$.

Figure 2(a) shows Mössbauer spectra of the frozen ferrofluid of coated 8 nm α-Fe_2O_3 nanoparticles with little interparticle interaction. In agreement with previous studies of ~8 nm α-Fe_2O_3 nanoparticles, where the interparticle interaction was negligible due to coating with oleic acid[18] or phosphate,[11] the spectra in Fig. 2(a) show a typical superparamagnetic behavior (i.e., a gradual transition from a sextet to a doublet in the temperature range 20–80 K, such that the relative area of the doublet gradually increases with increasing temperature). The superparamagnetic blocking temperature, T_B, defined as the temperature at which the sextet and the doublet have identical spectral areas, is around 70 K. At low temperatures, the sextet spectra show, as expected for nanoparticles with no Morin transition, a quadrupole shift, ε, of -0.10 mm/s. At $T \geqslant 180$ K, all the particles are superparamagnetic.

Figure 2(b) shows spectra of the freeze-dried sample of uncoated α-Fe_2O_3 particles. These spectra are magnetically split at 80 K and even at room temperature, but the absorption lines are substantially broadened and asymmetric above 80 K. This behavior is typical for samples of strongly interacting nanoparticles.[8–11,18] The temperature dependence of such spectra can be described by a mean field model for interacting nanoparticles.[8,23,26,27] The data in Fig. 2(b) also show that there is no Morin transition in these nanoparticles. We fitted the spectra obtained at temperatures $\leqslant 50$ K with a sextet [see the spectrum at 20 K in Fig. 2(b)] and found that the quadrupole shift, ε, of the interacting α-Fe_2O_3 nanoparticles is -0.085 mm/s. This is close to the value of -0.10 mm/s found both in bulk above T_M and in noninteracting α-Fe_2O_3 nanoparticles [Fig. 2(b)]. The uncertainty of ε is typically around 0.003 mm/s for sextet spectra with well-defined lines, as in those obtained at 25 and 20 K in Figs. 2(a) and 2(b), respectively.[17] The small difference in ε of ~0.015 mm/s between the ferrofluid and the dried sample has been explained by a rotation of the spin structure by an angle of ~15° ($\theta = 75^\circ$) that is induced by interparticle interactions in dried samples, where the easy axis of magnetizations of neighboring particles or chains of particles are nonparallel.[17]

Figure 2(c) shows Mössbauer data of α-Fe_2O_3 in the α-Fe_2O_3/NiO nanocomposite. In contrast to Figs. 2(a) and 2(b), the low-temperature spectrum (20 K) shows a positive quadrupole shift (the distance between lines 5 and 6 is larger than the distance between lines 1 and 2). At low temperatures (20–50 K), and more pronounced at intermediate temperatures (80–120 K), the spectra are asymmetric (e.g., lines 2 and 6 are

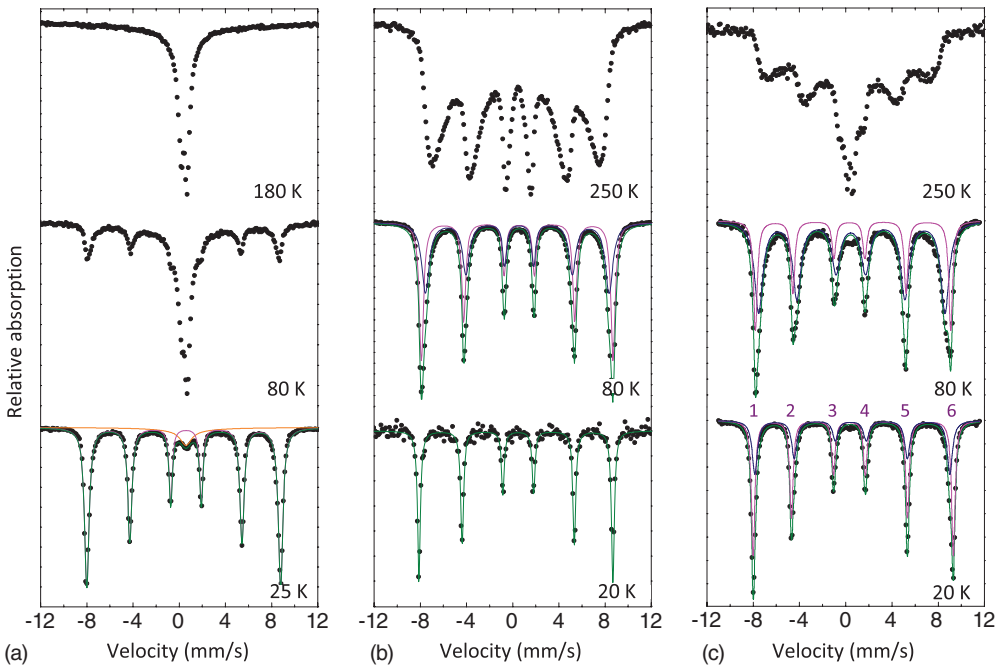

FIG. 2. (Color online) Mössbauer spectra of 8-nm α-Fe_2O_3 nanoparticles obtained at the indicated temperatures; (a) ferrofluid sample, (b) powder sample, and (c) mixed with NiO nanoparticles. The magenta/light gray numbers in panel c show how the lines are numbered. The solid (magenta/light gray and blue/dark gray) lines in panel b, at 80 K, and in panel c, at 20 K and 80 K, represent fits to the data by two sextets (sextets 1 and 2); the green/gray solid line is the sum of the fit components. The data in panel a at 25 K are fitted with one sextet and a doublet (orange/light gray), due to particles with fast superparamagnetic relaxation. The data in panel b obtained at 20 K are fitted with one sextet. The fit results for all the sextet components in panels a–c are summarized in Table I.

TABLE I. Mössbauer parameters obtained for α-Fe_2O_3 by fitting with one or two sextets the low-temperature spectra of the α-Fe_2O_3 ferrofluid sample (α-Fe_2O_3 (ff)), the α-Fe_2O_3 nanoparticle powder sample (α-Fe_2O_3 (fd)), and the α-Fe_2O_3 nanoparticles mixed with NiO nanoparticles (α-Fe_2O_3/NiO). The uncertainties of the given values for the hyperfine field (B_{hf}), isomer shift (δ), and quadrupole shift (ε) are ± 0.5 T, ± 0.02 mm/s, and ± 0.02 mm/s, respectively. The spectra are fitted with the area constraint that the sextet lines have the relative area distribution of 3:2:1:1:2:3 and that the line intensities and widths are pairwise equal. The line width (Γ^*) given in the table is an average value obtained by fitting the six lines in each sextet with the same line width.

Sample	T (K)	B_{hf} (T)	δ (mm/s)	ε (mm/s)	Γ^* (mm/s)
α-Fe_2O_3 (ff)	25	52.0	0.49	−0.10	0.45
α-Fe_2O_3 (fd)	20	52.5	0.49	−0.09	0.39
α-Fe_2O_3 (fd)	80	51.5	0.48	−0.09	0.42
		49.3	0.48	−0.08	0.64
α-Fe_2O_3/NiO	20	53.7	0.49	+0.16	0.36
		52.1	0.49	+0.08	0.49
α-Fe_2O_3/NiO	80	52.3	0.49	+0.15	0.42
		49.9	0.49	+0.04	0.75

broader and less intense than lines 5 and 1, respectively). This shows that Fe^{3+} ions are present in environments with different hyperfine interactions. The Mössbauer parameters obtained from fitting the low-temperature measurements in Fig. 2 are summarized in Table I.

The simplest but still sufficient fit of the Mössbauer data of α-Fe_2O_3/NiO in the range 20–130 K is composed of two sextets. The fits of the spectra obtained at 20 and 80 K are shown in Fig. 2(c). Fitting the data with just two sextets is only possible up to around 130 K; at higher temperatures, the spectra are too severely influenced by relaxation phenomena (seen as an increase in line width and from the occurrence of a doublet in the central part of the spectra at $T \gtrsim 80$ K). The quadrupole shifts, ε, of the two fitted sextets as a function of temperature are plotted in Fig. 3. At 20 K, one sextet with a relative spectral area of 65% has $\varepsilon = +0.16 \pm 0.02$ mms^{-1}. This corresponds to a spin direction with $\theta \approx 21^\circ$ (i.e., an out-of-plane spin rotation of $\approx 69^\circ$) in part of the α-Fe_2O_3 nanoparticle sample. The other sextet (with a relative spectral area of 35% at 20 K) has a quadrupole shift of $\varepsilon = +0.08 \pm 0.02$ mm/s, corresponding to $\theta \approx 39^\circ$. At increasing temperature, the quadrupole shifts of both sextets decrease, and at 130 K, the ε-values are close to 0.00 mm/s for both sextets (Fig. 3). We have considered other fitting procedures than using two sextets and found that they produced qualitatively similar results (i.e., untypical ε-values in the range of around +0.16–0.00 mm/s are still obtained) or they give less good fits. The spectra cannot be described solely by a superposition of two sextets for α-Fe_2O_3 being truly above and below the Morin transition. The fact that we get two spin directions, θ, of 21° and 39° is most likely a consequence of fitting with two sextets rather than the spin orientation being preferentially in these two specific directions. Correspondingly, fitting with three sextets gives three spin directions ($\neq 0^\circ$, 90°). Presumably there is a distribution of spin orientations around the mean value of $\theta = 27^\circ$.

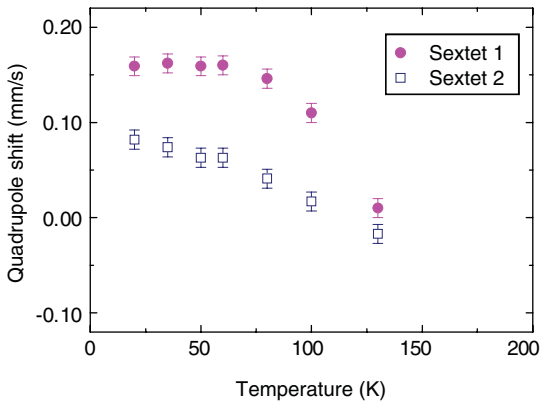

FIG. 3. (Color online) The quadrupole shift of the two sextet components (sextet 1 (filled circles) and sextet 2 (open squares)) in the Mössbauer spectra of the α-Fe_2O_3/NiO nanoparticles as a function of temperature.

The doublet present in the Mössbauer spectra of α-Fe_2O_3/NiO at $T > 80$ K [Fig. 2(c), 250 K] also indicates that the magnetic relaxation is faster for some of the α-Fe_2O_3 particles mixed with NiO particles compared with the pure uncoated α-Fe_2O_3 sample [Fig. 2(b)], which display only a sextet at the same temperatures. However, the relaxation is still considerably slower compared with the ferrofluid sample [Fig. 2(a)].

B. Neutron diffraction

Neutron powder diffraction is another useful technique to obtain information about spin rotation in α-Fe_2O_3 relative to the [001] axis. In neutron diffraction data, the dominant contribution to the intensity originating from magnetic scattering is given by the magnetic structure factor, which is proportional to the component of the magnetic moment $\vec{\mu}$ perpendicular to the scattering vector $\vec{q}$. Therefore, for α-Fe_2O_3 the intensity of the magnetic (003) reflection has its maximum when the spins are perpendicular to the [001] axis and almost vanishes when the spins become parallel to the [001] axis.[28] We can write the variation in intensity I as a function of the angle γ between $\vec{\mu}$ and $\vec{q}$ as

$$I(\vec{q},T) = c(\vec{q},T)\mu^2 \sin^2 \gamma(\vec{q}), \tag{4}$$

where, for $\vec{q} = [003]$ in hematite and $\gamma(\vec{q})$is the polar angle between the magnetic moment and the [001] axis (i.e., $\gamma(\vec{q} = [003]) = \theta$ used in Eq. (3)). Within the prefactor $c(\vec{q},T)$ is included the square of the magnetic structure and form factors, which depend on the scatting vector $\vec{q}$, and the Debye–Waller factor, which depends on $\vec{q}$ and T.

Neutron diffraction data for the dried sample of α-Fe_2O_3 nanoparticles are shown in Fig. 4(a). We have subtracted a linear background and fitted the data with four Lorentzian lines. Within uncertainty, no change is observed for the integrated intensities (the areas) of the reflections in the studied temperature range of 20–300 K (i.e., no spin rotation is observed). The integrated intensities at all measured temperatures (20–300 K) of the magnetic (003) and (101) reflections scaled to that of the structural (104) reflection are

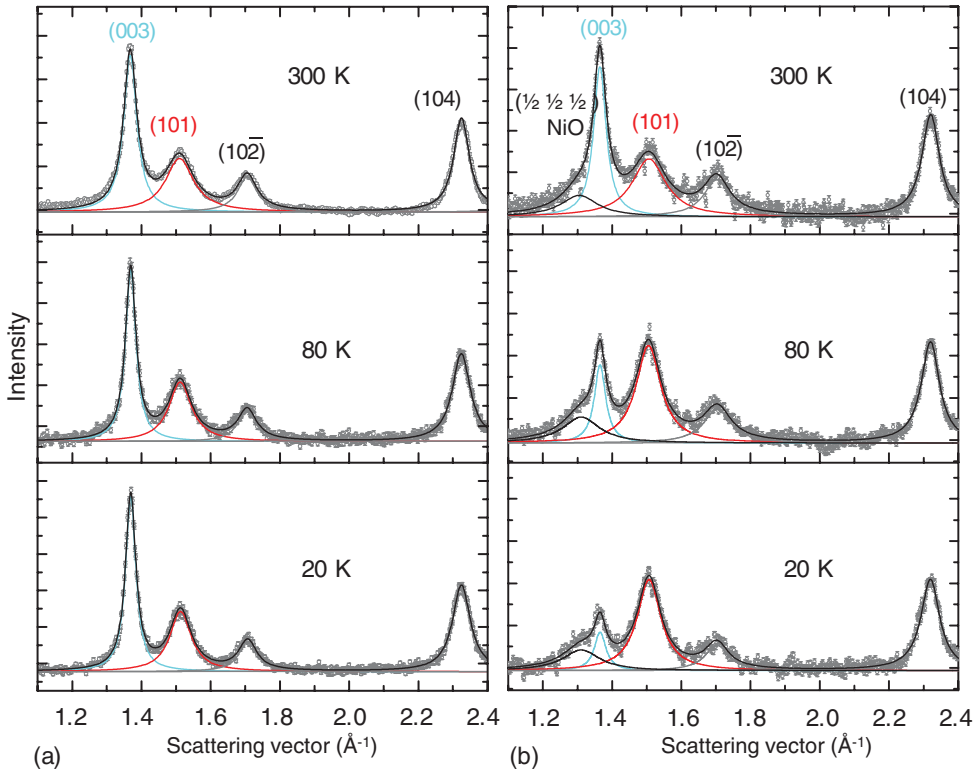

FIG. 4. (Color online) Neutron powder diffraction data obtained at 20, 80, and 300 K of (a) 8-nm α-Fe_2O_3 particles and (b) α-Fe_2O_3/NiO nanoparticles. The solid lines are fits to data with Lorentzian lines and a background with constant slope.

$I_F(003) = 0.81 \pm 0.02$ and $I_F(101) = 0.60 \pm 0.02$ (the indices F denote that these results are from the pure α-Fe_2O_3 sample).

Neutron diffraction data of the composite α-Fe_2O_3/NiO nanoparticle sample are shown in Fig. 4(b). It is apparent from the changing intensities of the magnetic (003) and (101) reflections that a large spin rotation occurs in α-Fe_2O_3 at low temperatures. We have applied the same fitting procedure as above but included an extra Lorentzian line to account for the only NiO reflection within the data range, the antiferromagnetic $(\frac{1}{2}\frac{1}{2}\frac{1}{2})$ reflection of NiO observed at around $q = 1.28$ Å^{-1}. The integrated intensities I_N of the magnetic (003) and (101) reflections in the α-Fe_2O_3/NiO composite scaled to that of the structural (104) reflection (where the indices N denote that these results are from the composite α-Fe_2O_3/NiO sample) are plotted in Fig. 5. This simple procedure for determining peak intensities is equivalent to using FullProf in the profile matching mode. It was adopted because a full structure refinement with FullProf of just one magnetic NiO peak and four hematite peaks (two nuclear and two magnetic) would need to be too constrained to be meaningful. Between ~180 K and 300 K, the values are close to those found for the pure α-Fe_2O_3 sample (indicated by the arrows in Fig. 5), but at temperatures below ~150 K, the (003) reflection decreases significantly in intensity, whereas the (101) reflection increases. At 20 K we find that the integrated intensity of the magnetic (003) reflection I_N scaled to the structural (104) reflection, is $I_N(003) = 0.19 \pm 0.02$ (Fig. 5). In the previous paragraph we found $I_F(003) = 0.81 \pm 0.02$ at 20 K, and we know from Mössbauer spectroscopy (Sec. III A) that this corresponds to $\theta_F \sim 75°$. If we assume that $c(\vec{q},T)$ and μ in Eq. (4) are the same for the (003) reflection of both samples at 20 K, we may write $I_N(003)/I_F(003) = \sin^2\theta_N/\sin^2\theta_F$ and thereby calculate the angle θ_N of the spin orientation relative to [001] of α-Fe_2O_3 in the composite at 20 K to be ~28°. This corresponds well to the Mössbauer results, in which we found (within the two-sextet model) that approximately 65% of the spins had an angle of 21° and 35% had one of 39° at 20 K, giving a mean value of 27°. Applying the same analysis to the 80 K Mössbauer spectroscopy and neutron diffraction data gives mean values of θ_N of ~37° and ~38°, respectively.

From the broadening of the magnetic (003) and (101) reflections it is possible to estimate the magnetic correlation lengths l_m perpendicular to the (001) and (101) planes as $l_m = 2\pi/(\mathrm{FWHM} - B_i)$, where B_i is the instrumental line broadening and FWHM is the Full Width at Half Maximum of the (003) and (101) reflections obtained from fitting data with Lorentzian lines. We find that the magnetic correlation lengths essentially remain unchanged across the spin rotation temperatures ($l_{m(003)} = 15 \pm 1$ nm and $l_{m(101)} = 6 \pm 1$ nm at 20 K), with values similar to those of the pure α-Fe_2O_3 sample ($l_{m(003)} = 14 \pm 1$ nm and $l_{m(101)} = 7 \pm 1$ nm). (In all the neutron diffraction data (Fig. 4), the (003) reflection is noticeably narrower than the (101) reflection. This is due to oriented attachment of some of the α-Fe_2O_3 particles into chains along the [001] direction, combined with formation of magnetic coherence between attached particles as described in detail in Ref. 9.) When comparing the magnetic correlation length to particle size analysis,[9] based on XRD measurements and TEM, we find that the magnetic correlation

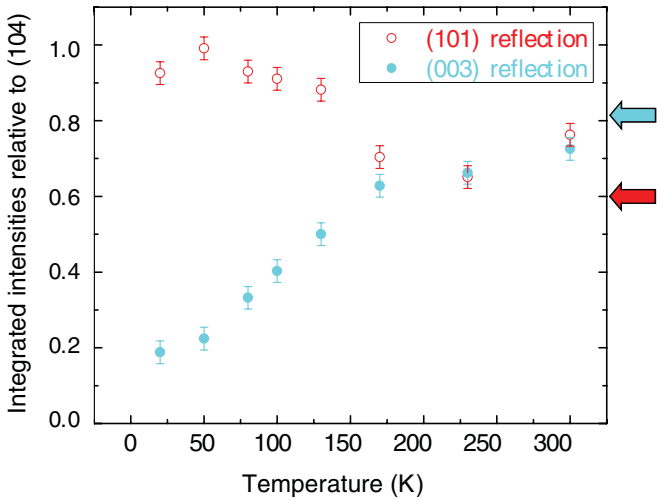

FIG. 5. (Color online) The integrated intensities of the magnetic reflections [(003), filled circles, and (101), open circles] of α-Fe_2O_3 nanoparticles mixed with NiO particles as a function of temperature. The integrated intensities are given relative to that of the structural (104) reflection. The cyan/medium gray and red/dark gray arrows to the right indicate the mean integrated intensities (scaled) of the (003) and (101) reflections, respectively, found for pure α-Fe_2O_3 nanoparticles at temperatures between 20 and 300 K.

length is similar to the crystalline correlation length (i.e., the α-Fe_2O_3 particles are single-domain at all temperatures), both in the pure α-Fe_2O_3 sample and the α-Fe_2O_3/NiO sample. This excludes the possibility that the α-Fe_2O_3 particles may have a multidomain-like magnetic structure, where the spin orientation in part of a particle is different from that in another part of the same particle. The absence of domain walls in the α-Fe_2O_3 nanoparticles in the α-Fe_2O_3/NiO composite is in good agreement with the general perception that nanoparticles are too small to have domains. Instead, it can be concluded that, because the particles are single-domain particles at all studied temperatures, the sublattice magnetizations of individual α-Fe_2O_3 particles rotate coherently out of the (001) plane.

IV. DISCUSSION

The Mössbauer and neutron diffraction data for the α-Fe_2O_3/NiO sample lead us to the following picture of the spin structure of the α-Fe_2O_3 nanoparticles in the composite. At low temperatures ($T = 20$ K), the sublattice magnetization directions of the individual particles are rotated coherently out of the (001) plane. The magnetization attains an average direction close to $\theta = 27^\circ$ at 20 K. With increasing temperature (50-180 K) the sublattice magnetization directions approach the (001) plane. Previously, distinct intermediate states ($\theta \neq 0^\circ, 90^\circ$) have been proposed to exist in Al-substituted bulk-like α-Fe_2O_3 during the Morin transition.[29,30] The spin rotation observed in α-Fe_2O_3/NiO has similarities with that observed in systems of interacting α-Fe_2O_3 nanoparticles[17] but it is much larger. In the following, we discuss exchange interaction between neighboring particles with different directions of easy axes as an origin of spin rotation with $\theta \neq 0^\circ, 90^\circ$.

A. Theoretical model for spin rotation in interacting nanoparticles

We first consider a simple example with two particles with uniaxial anisotropy at low temperatures, in which one sublattice of one particle interacts with one sublattice of the other particle. A schematic drawing of the two interacting particles, p and q, with anisotropy constants K_p and K_q and volumes V_p and V_q, respectively, is shown in Fig. 6. Here, the easy axes, $\vec{e}_p$ and $\vec{e}_q$ of the two particles form an angle α. Because of the exchange interaction at the interface, the sublattice magnetization directions $\vec{M}_p$ and $\vec{M}_q$ are rotated by the angles θ_p and θ_q, respectively. For simplicity, we consider only one sublattice of particle p interacting with one sublattice of particle q, and we assume that the exchange interactions between surface spin of neighboring particles result in an interaction energy given by Eq. (2). The magnetic energy may then be written as

$$E(\theta_p,\theta_q) = K_pV_p \sin^2\theta_p + K_qV_q \sin^2\theta_q - J_{\text{eff}}\, M_pM_q\, \cos(\alpha - \theta_p - \theta_q) \quad (5)$$

where the first two terms are the anisotropy energies of particles p and q, and the last term represents the effective exchange interaction between the two particles. To find energy minima, Eq. (5) is differentiated with respect to θ_p and θ_q, and we obtain

$$\frac{\partial E}{\partial \theta_p} = 2K_pV_p \sin\theta_p \cos\theta_p + J_{\text{eff}}\, M_p\, M_q \times \sin(\alpha - \theta_p - \theta_q) = 0 \quad (6)$$

and

$$\frac{\partial E}{\partial \theta_q} = 2K_qV_q \sin\theta_q \cos\theta_q + J_{\text{eff}}\, M_p\, M_q \times \sin(\alpha - \theta_p - \theta_q) = 0, \quad (7)$$

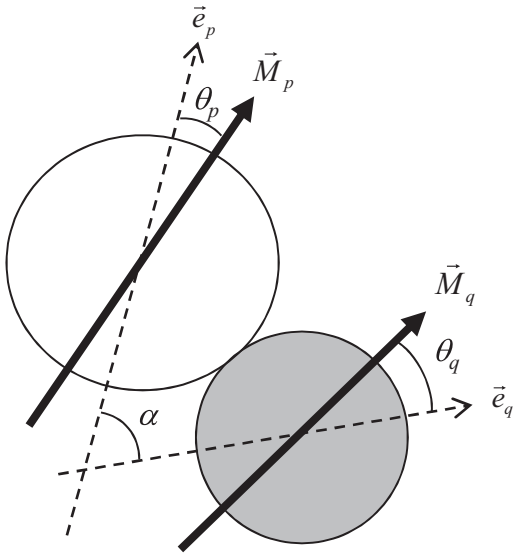

FIG. 6. Schematic illustration of two interacting nanoparticles with easy axes $\vec{e}_p$ and $\vec{e}_q$ and sublattice magnetization directions $\vec{M}_p$ and $\vec{M}_q$. α is the angle between the two easy axes, and θ_p and θ_q denote the angles between the easy axes and the sublattice magnetization of the two particles.

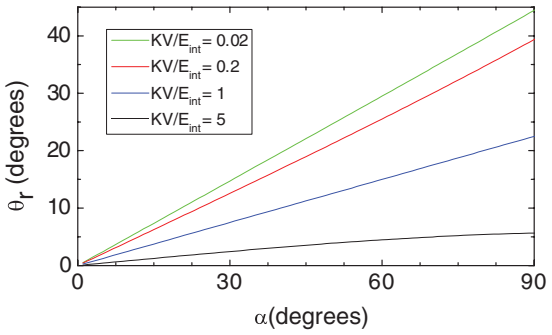

FIG. 7. (Color online) The dependence of θ_r as a function of α, as given by Eq. (10), for $KV/E_{\rm int} = 0.02$, 0.2, 1, and 5.

from which we find

$$\sin 2\theta_q = \frac{K_p\, V_p}{K_q\, V_q} \sin 2\theta_p. \tag{8}$$

Inserting Eq. (8) into Eq. (6), we obtain

$$K_p V_p \sin 2\theta_p - J_{\rm eff} M_p\, M_q \times \sin\left[\alpha - \theta_p - \frac{1}{2}\arcsin\left(\frac{K_p\, V_p}{K_q\, V_q}\sin 2\theta_p\right)\right] = 0, \tag{9}$$

which may be solved numerically to obtain values of θ_p for given values of the magnetic anisotropy energies, the angle α, and the interaction energy, $E_{\rm int} = J_{\rm eff}\, M_p\, M_q$.

To illustrate the effects of interactions, we consider the simple case where $K_p\, V_p = K_q\, V_q \equiv KV$, for which one can find an analytical solution for the rotation angle $\theta_p = \theta_q \equiv \theta_r$,

$$\cot 2\theta_r = \frac{KV}{E_{\rm int}\sin\alpha} + \cot\alpha. \tag{10}$$

The dependence of θ_r as a function of α for $KV/E_{\rm int} = 0.02$, 0.2, 1, and 5 is shown in Fig. 7. If the easy axes of the two particles are parallel ($\alpha = 0^\circ$), one finds the intuitive result $\theta_r = 0^\circ$, irrespective of the strength of the interaction energy. However, if the interaction energy is large compared with the anisotropy energy, and the value of the angle α is large, the rotation angle θ will be large at low temperatures. In the above calculations we assumed that $K_pV_p = K_qV_q$, and therefore the rotation angle is the same in both particles, and the maximum rotation is 45° when $\alpha = 90^\circ$. In cases where $K_pV_p > K_qV_q$, rotation angles up to 90° may exist in particle q.

At higher temperatures, the sublattice magnetization directions perform fast fluctuations around the directions corresponding to the energy minima.[8,26,27] Therefore, M_p and M_q should be replaced by the thermal averages $\langle M_p\rangle$ and $\langle M_q\rangle$ such that the interaction energy is given by $E_{\rm int} = J_{\rm eff}\langle M_p\rangle\langle M_q\rangle$. With increasing temperature, $\langle M_p\rangle$ and $\langle M_q\rangle$ decrease, leading to an increase of cot $2\theta_r$, i.e. a decrease of the spin rotation angle.

B. The α-Fe_2O_3/NiO composite

The assumption of simple uniaxial anisotropy in the above calculations is not fulfilled in the α-Fe_2O_3/NiO system. Hematite nanoparticles have a large uniaxial anisotropy for rotations out of the hexagonal (001) plane and a much smaller anisotropy for rotations within the (001) plane.[20,31,32] The anisotropy of bulk NiO with an fcc structure is also quite complex,[28] with the spins confined in the (111) plane due to a large out-of-plane anisotropy, and the easy direction is in the [11$\bar{2}$] direction within the (111) plane,[22] but the anisotropy in nanoparticles may be different from that of bulk NiO. Moreover, in the model described in Sec. IV A, only interactions between two particles are considered, but in a sample of interacting nanoparticles it is most likely that each particle interacts with more than one neighboring particle. However, the simple model can be used to obtain a qualitative understanding of the influence of interactions on the spin structure in systems of nanoparticles.

According to the model, the relative size of the anisotropy energies of the interacting particles and the interaction energy are important parameters. In α-Fe_2O_3 nanoparticles, the out-of plane anisotropy constant is on the order of 10^4–10^5 Jm^{-3}.[21] In 8-nm hematite particles, this corresponds to an anisotropy energy on the order of 200–2000 K. Using the bulk value for the out-of-plane anisotropy constant of NiO ($K_1 \cong 4.3 \times 10^5$ Jm^{-3}),[33] one finds that for the NiO nanoparticles, the anisotropy energy K_1V_1 is around 9000 K.[13] Mössbauer studies of samples of strongly interacting pure α-Fe_2O_3 and pure NiO particles yielded interaction energies $J_{\rm eff}M_pM_q$ for ensembles of particles on the order of 600 K[17] and 360 K,[13] respectively. Similarly, studies of the α-Fe_2O_3/NiO composite[18] indicate interaction energies on the same order of magnitude.

Based on the model discussed in Sec. IV A, the large rotation angles at low temperatures indicate that the easy axes of the NiO nanoparticles form large angles, α, with the easy axis within the (001) plane of the majority of the α-Fe_2O_3 nanoparticles and may be close to being perpendicular to this. The apparent absence of small rotation angles at low temperatures suggests that the easy axes of neighboring α-Fe_2O_3 and NiO particles are not completely randomly oriented relative to each other. Assuming that the angle α between the easy axes of neighboring particles has a preferred value might seem too simplistic, considering the random orientation of the easy axes one might expect for particles in a powder. However, oriented attachment between nanoparticles of the same material has been observed in numerous systems and is considered to be a mechanism for crystal growth.[34,35] Correspondingly, there is nothing fundamental that prevents epitaxial assembly of particles of different materials to occur under the right conditions, and therefore it is possible that the particles in the α-Fe_2O_3/NiO system might have a tendency to assemble with a preferred orientation when mixed in water and subsequently dried. Epitaxial assembly of NiO and α-Fe_2O_3 can be obtained if the close-packed oxygen structure in the two materials is continued across their interface, such that the [001] axis and a [100] axis of α-Fe_2O_3 are parallel to a [111] axis and a [11$\bar{2}$] axis of NiO, respectively, as illustrated in Fig. 8. In this case, the antiferromagnetic modulation vectors along [001] of α-Fe_2O_3 and [111] of NiO can be parallel, too, and hence the antiferromagnetic modulation can continue across the epitaxial assembly at the particle interface.

Because the relative spatial orientation of the particles is crucial for understanding the spin reorientation, TEM can give useful information. TEM has to date been the key

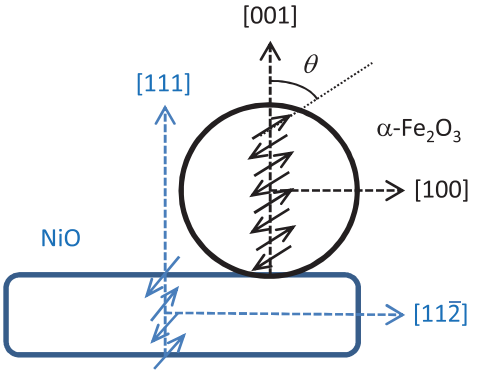

FIG. 8. (Color online) Schematic illustration of epitaxial attachment of α-Fe_2O_3 and NiO nanoparticles.

technique to verify oriented attachment.[34,35] However, we found it difficult to obtain micrographs that could resolve the particle attachment on composite samples. TEM imaging gives a two-dimensional (2D) projection of the aggregated crystals; therefore, to obtain useful images, the aggregates must have a 2D rather than a 3D complexity. In the case of a composite, it is also somewhat rare to get neighboring particles aligned such that two sets of lattice planes of each particle are visible, as needed for fully establishing crystal orientations. Existence of similar lattice spacings in α-Fe_2O_3 and NiO further complicates the image interpretation. However, the different morphologies of α-Fe_2O_3 (spherical) and NiO (plate-shaped) nanoparticles helped image interpretation. A few examples of aggregated α-Fe_2O_3 and NiO nanoparticles, from which the particle orientations can be established, are shown in Figs. 9(b) and 9(c). The images suggest the existence of preferred attachment of α-Fe_2O_3 and NiO nanoparticles.

An energy-filtered TEM image [Fig. 9(a)] of the rim of a larger aggregate shows that the α-Fe_2O_3 and NiO nanoparticles are intimately mixed at a scale of $\leqslant\sim$20 nm. In Fig. 9(b), a high-resolution bright field image of an agglomerate of at least 14 particles is seen. In the center of this image is a thick nanoparticle (white dashed outline), which is recognized as NiO from its (plate) shape, and 2.4-Å lattice fringes, representing (111) planes, parallel to the plane of the particle. Next to this particle, is another large nanoparticle (black dashed outline), which shows a lattice spacing of 1.46 Å (see enlargement of area in red square). These are presumably (030) planes of α-Fe_2O_3. It can be seen from the fast Fourier transform (FFT) of the red square image that the (111) planes of NiO are perpendicular to the (030) planes of α-Fe_2O_3 (i.e., it is a possibility that the [111] axis of NiO is parallel to [001] axis of α-Fe_2O_3). The nanoparticles (white outlines) in the lower half of the image are NiO particles seen from other angles; their plate shapes make $\sim$70° angles with the plate shape of the large NiO particle in the center. In the upper, right part of Fig. 9(b), there appear to be two chain-like assemblies of three α-Fe_2O_3 particles each. In the upper chain (dashed black outlines), the [001] axis (dashed arrow) is determined from a set of two different lattice planes. In the lower α-Fe_2O_3 chain (black outlines), only one set of lattice planes is seen, and it is difficult to determine the orientation of the [001] axis, but if we assume that the [001] axis is preferentially oriented parallel to the length of the chain (as found in Ref. 9), then the [001] axis of this chain (indicated by a solid arrow) appears to be at an angle of 10° relative to that of the other chain. The attachment between the NiO particle in the center and the α-Fe_2O_3 particles in the upper right corner does not seem to have the suggested epitaxial attachment, but the particles may still find the expected arrangement locally. The (111) planes of the small NiO plate (thick white outline) are at an angle close to 90° to the [001] axes of the α-Fe_2O_3 chains. In Fig. 9(c), an image case very similar to that in the center of Fig. 9(b) is seen. Figure 9(c) shows a nanoparticle with lattice spacing of 1.47 Å perpendicular to the 2.4-Å lattice spacing (the (111) planes) of the small agglomerate of NiO nanoparticles (white outlines) next to it. Thus, in the TEM images, there are examples giving the possibility that the particles are attached such that the [001] axis of α-Fe_2O_3 is parallel to the [111] axis of NiO, but variations exists. Despite the complexity of such studies, further TEM studies are desirable to quantify fully the attachment of nanoparticles of different materials.

Given that the α-Fe_2O_3 and NiO nanoparticles have a tendency to attach with preferred epitaxial orientation, as described above (Fig. 8), the large rotation of the sublattice magnetization out of the (001) plane in the α-Fe_2O_3 nanoparticles suggests that the sublattice magnetization directions of the neighboring NiO nanoparticles are not in the NiO (111) plane parallel to the faces of the disc-shaped particles and may form a large angle with this plane. Neutron powder diffraction of NiO nanoparticles has recently been applied to reveal the spin direction relative to the (111) particle plane.[36] Numerous studies of ferromagnetic thin films have shown that there is commonly a spin reorientation transition such that the magnetization is perpendicular to the film plane below a critical film thickness, but within the film plane for larger film thickness. The perpendicular magnetization in very thin films can be explained by a strong magnetic anisotropy perpendicular to the film plane, because surface anisotropy becomes predominant compared with other contributions to the magnetic anisotropy.[37] The critical film thickness is temperature dependent and can be on the order of three to 10 monolayers. A similar spin reorientation transition can also be found in antiferromagnetic thin films,[38] and thus it is possible that plate-shaped NiO particles with a thickness of only 2 nm also have a large surface anisotropy, which may favor the sublattice magnetization to form a large angle to the surface plane. The faces of the disc-shaped NiO particles are (111) planes,[13] but in the fcc structure, there are four equivalent (111) planes, the three others forming angles of 70.5° to this. It is likely that the surface anisotropy will favor sublattice magnetization directions within or close to one of these (111) planes.

With the configuration of particle attachment described above, the spin direction in α-Fe_2O_3 is at a large angle to the α-Fe_2O_3/NiO interface plane, and the spins in α-Fe_2O_3 tend to align with the spin direction in NiO. This spin configuration is different from the perpendicular coupling explained by Koon,[5] in which the sublattice magnetization directions of the two constituents are perpendicular, but remain parallel to the interface layer.

The temperature dependence of the quadrupole splitting, shown in Fig. 3, as well as the temperature dependence of the areas of the diffraction peaks, shown in Fig. 5, indicates a

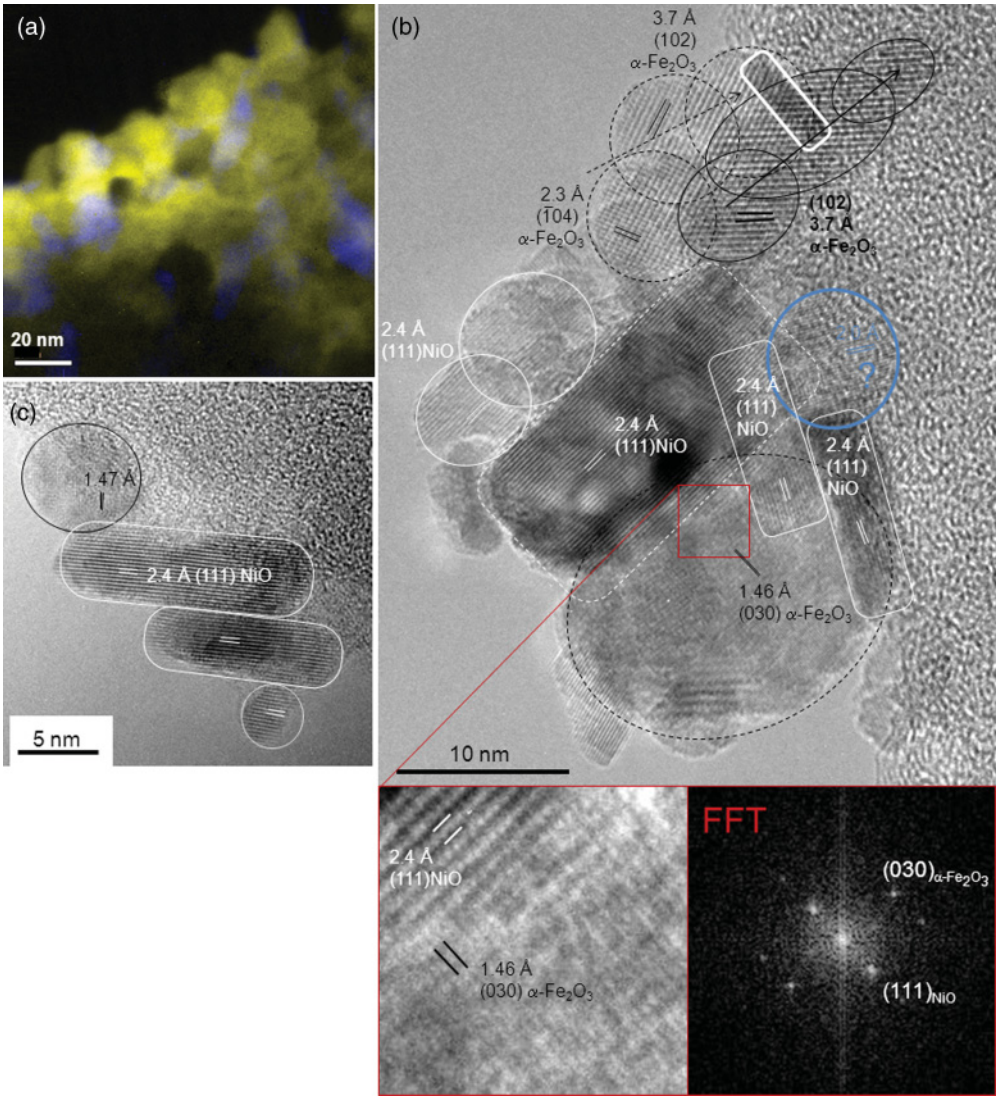

FIG. 9. (Color online) TEM images of α-Fe_2O_3/NiO nanoparticle composite. (a) Elemental map of aggregate of α-Fe_2O_3 and NiO particles. Blue/medium gray and yellow/light gray represent enrichment in iron (α-Fe_2O_3) and nickel (NiO), respectively. (b, c) TEM images of assemblies of more than 14 particles and of four particles, respectively. α-Fe_2O_3 nanoparticles are indicated by black outlines and NiO nanoparticles by white outlines. The lower panels in panel b show an enlargement of the area with red/dark gray outline and the fast Fourier transform (FFT) of this. The particle with a blue/medium gray outline in panel b is not identified (lattice plane spacings correspond to both α-Fe_2O_3 and NiO).

decrease of the rotation angle with increasing temperature. This can be explained by the decrease of the averaged sublattice magnetizations $\langle M_p \rangle$ and $\langle M_q \rangle$ with increasing temperature, as discussed in Sec. IV A.

C. Comparison with α-Fe_2O_3/CoO

In composites of α-Fe_2O_3 and CoO nanoparticles, the relaxation of the α-Fe_2O_3 nanoparticles is suppressed much more than in the α-Fe_2O_3/NiO samples, indicating a very strong interparticle interaction.[18] At first sight, it may therefore appear surprising, that the spin rotation is much smaller in the α-Fe_2O_3/CoO composite. In fact, the quadrupole shift of the α-Fe_2O_3 nanoparticles is identical to the bulk value above the Morin transition temperature ($\varepsilon = -0.100$ mm/s). Therefore, it seems that the easy axes of the CoO nanoparticles are parallel to the (001) plane of the α-Fe_2O_3 particles. If a hematite nanoparticle is attached to a CoO particle with easy axis parallel to the (001) plane of hematite, the exchange energy can be minimized by rotation of the sublattice magnetization of hematite within the (001) plane. This would not result in any change of either the quadrupole shift in the Mössbauer spectra or of the intensity of the (003) reflection in neutron powder diffraction. Such a parallel (or antiparallel) orientation of the sublattice magnetization directions will also minimize the interparticle exchange coupling energy [Eq. (2)].

V. CONCLUSIONS

By use of Mössbauer spectroscopy, neutron diffraction, and transmission electron microscopy, we have investigated

the spin orientation in α-Fe_2O_3 nanoparticles mixed with nanoparticles of other antiferromagnetic materials. It is shown that when α-Fe_2O_3 nanoparticles are wet-mixed with NiO nanoparticles and subsequently dried, a spin reorientation transition somewhat similar to the Morin transition can be induced in the α-Fe_2O_3 particles. However, in contrast to bulk, where the Morin transition is caused by intrinsic anisotropy in α-Fe_2O_3, the spin reorientation in the α-Fe_2O_3 nanoparticles is caused by exchange coupling to the NiO particles with a different direction of easy axis. The spin rotation angle decreases with increasing temperature. This can be explained by a decrease in the average sublattice magnetization. The results presented above on α-Fe_2O_3/NiO, and compared with data on α-Fe_2O_3 and α-Fe_2O_3/CoO, suggest that nanoparticles of different types of materials can be assembled epitaxially and that this has a strong influence on their magnetic properties and, in particular, their spin orientation. It is possible that the assembly can be exploited as a way to construct and tailor, on a larger scale, composites of magnetic materials with new properties.

ACKNOWLEDGMENTS

We thank the Danish Council for Independent Research, Technology, and Production Sciences and Natural Sciences (Steno stipend (C.F.) and DanScatt) for funding. The neutron scattering measurements were performed at the Swiss Spallation Neutron Source, SINQ, Paul Scherrer Institute, Villigen, Switzerland.

*fraca@fysik.dtu.dk
†Present address: SimCorp A/S, DK-2300 Copenhagen S, Denmark.
‡Present address: Department of Materials, University of Oxford, Oxford, OX1 3PH, UK.

[1] W. H. Meiklejohn and C. P. Bean, Phys. Rev. **102**, 1413 (1956).
[2] A. E. Berkowitz and K. Takano, J. Magn. Magn. Mater. **200**, 552 (1999).
[3] J. Noqués and I. Schuller, J. Magn. Magn. Mater. **192**, 203 (1999).
[4] J. Noqués, J. Sort, V. Skumryev, S. Suriñach, J. S. Muñoz, and M. D. Baró, Physics Reports **442**, 65 (2005).
[5] N. C. Koon, Phys. Rev. Lett. **78**, 4865 (1997).
[6] Y. Ijiri, T. C. Schulthess, J. A. Borchers, P. J. van der Zaag, and R. W. Erwin, Phys. Rev. Lett. **99**, 147201 (2007).
[7] S. Mørup, M. F. Hansen, and C. Frandsen, Beilstein J. Nanotechnol. **1**, 182 (2010).
[8] M. F. Hansen, C. B. Koch, and S. Mørup, Phys. Rev. B **62**, 1124 (2000).
[9] C. Frandsen, C. R. H. Bahl, B. Lebech, K. Lefmann, L. Theil Kuhn, L. Keller, N. H. Andersen, M. v. Zimmermann, E. Johnson, S. N. Klausen, and S. Mørup, Phys. Rev. B **72**, 214406 (2005).
[10] C. Frandsen and S. Mørup, J. Phys.: Condens. Matter **18**, 7079 (2006).
[11] L. Theil Kuhn, K. Lefmann, C. R. H. Bahl, S. N. Ancona, P.-A. Lindgård, C. Frandsen, D. E. Madsen, and S. Mørup, Phys. Rev. B **74**, 184406 (2006).
[12] F. Bødker, M. F. Hansen, C. B. Koch, and S. Mørup, J. Magn. Magn. Mater. **221**, 32 (2000).
[13] C. R. H. Bahl, K. Lefmann, L. T. Kuhn, N. B. Christensen, H. Vásquez, and S. Mørup, J. Phys.: Condens. Matter **18**, 11203 (2006).
[14] C. R. H. Bahl and S. Mørup, Nanotechnology **17**, 2835 (2006).
[15] T. S. Berquó, J. J. Erbs, A. Lindquist, R. L. Penn, and S. K. Banerjee, J. Phys. Condens. Matter **21**, 176005 (2009).
[16] M. Xu, C. R. H. Bahl, C. Frandsen, and S. Mørup, J. Colloid Interface Sci. **279**, 132 (2004).
[17] C. Frandsen and S. Mørup, Phys. Rev. Lett. **94**, 027202 (2005).
[18] C. Frandsen and S. Mørup, J. Magn. Magn. Mater. **266**, 36 (2003).
[19] L. Wang and L. Gao, J. Colloid Interface Sci. **349**, 519 (2010).
[20] A. H. Morrish, *Canted Antiferromagnetism: Hematite* (World Scientific, Singapore, 1994).
[21] F. Bødker and S. Mørup, Europhys. Lett. **52**, 217 (2000).
[22] W. L. Roth, Phys. Rev. **110**, 1333 (1958).
[23] S. Mørup, D. E. Madsen, C. Frandsen, C. R. H. Bahl, and M. F. Hansen, J. Phys.: Condens. Matter **19**, 213202 (2007).
[24] S. Mørup and C. W. Ostenfeld, Hyperfine Interact. C **5**, 83 (2002).
[25] T. Sugimoto, Y. Wang, H. Itoh, and A. Muramatsu, Colloid. Surf. A **134**, 265 (1998).
[26] S. Mørup, M. B. Madsen, J. Franck, J. Villadsen, and C. J.W Koch, J. Magn. Magn. Mater. **40**, 163 (1983).
[27] D. E. Madsen, L. Cervera-Gontard, T. Kasama, R. E. Dunin-Borkowski, C. B. Koch, M. F. Hansen, C. Frandsen, and S. Mørup, J. Phys.: Condens. Matter **21**, 016007 (2009).
[28] C. G. Shull, W. A. Strauser, and E. O. Wollan, Phys. Rev. **83**, 333 (1951).
[29] R. E. Vandenberghe, E. Van San, and E. De Grave, Hyperfine Interact. C **5**, 209 (2002).
[30] R. E. Vandenberghe, E. Van San, E. De Grave, and G. M. Da Costa, Czech. J. Phys. **51**, 663 (2001).
[31] F. Bødker, M. F. Hansen, C. B. Koch, K. Lefmann, and S. Mørup, Phys. Rev. B **61**, 6826 (2000).
[32] S. N. Klausen, K. Lefmann, P.-A. Lindgård, L. Theil Kuhn, C. R. H. Bahl, C. Frandsen, S. Mørup, B. Roessli, N. Cavadini, and C. Niedermayer, Phys. Rev. B **70**, 214411 (2004).
[33] M. T. Hutchings and E. J. Samuelsen, Phys. Rev. B **6**, 3447 (1972).
[34] R. L. Penn and J. F. Banfield, Geochim. Cosmochim. Acta **63**, 1549 (1999).
[35] J. F. Banfield, S. A. Welch, H. Zhang, T. T. Ebert, and R. L. Penn, Science **289**, 751 (2000).
[36] E. Brok, B. Lebech, K. Lefmann, and C. Frandsen, 5th European Conference on Neutron Scattering, Prague, Abstract **EM24-118** (2011).
[37] P. E. Jensen and K. H. Bennemann, Surf. Sci. Reports **61**, 129 (2006).
[38] D. S. Deng, X. F. Jin, and R. Tao, Phys. Rev. B **69**, 172403 (2004).